Heliyon 10 (2024) e37227

Contents lists available at ScienceDirect

Heliyon

journal homepage: www.cell.com/heliyon

Research article

Molecular basis of CX-5461-induced DNA damage response in primary vascular smooth muscle cells

Tengfei Liu [a,b], Guopin Pan [c], Jing Zhang [d,1], Jianli Wang [e,**], Xiaosun Guo [d], Ye Chen [d,2], Xiaoyun Wang [d], Xiaopei Cui [b], Huiqing Liu [a,***], Fan Jiang [b,*]

[a] *Department of Pharmacology, School of Basic Medical Sciences, Cheeloo College of Medicine, Shandong University, Jinan, Shandong Province, China*

[b] *Gerontology and Anti-Aging Research Laboratory, Department of Geriatric Medicine, Qilu Hospital of Shandong University, Jinan, Shandong Province, China*

[c] *College of Pharmacy, Henan International Joint Laboratory of Cardiovascular Remodeling and Drug Intervention, Xinxiang Key Laboratory of Vascular Remodeling Intervention and Molecular Targeted Therapy Drug Development, Xinxiang Medical University, Xinxiang, Henan Province, China*

[d] *Department of Physiology and Pathophysiology, School of Basic Medical Sciences, Cheeloo College of Medicine, Shandong University, Jinan, Shandong Province, China*

[e] *Department of Obstetrics and Gynecology, Qilu Hospital of Shandong University, Jinan, Shandong Province, China*

ARTICLE INFO

Keywords:
CX-5461
DNA damage response
Replication stress
Nucleolus
ATM/ATR
p53
Vascular smooth muscle cell

ABSTRACT

Our previous studies have shown that the novel selective RNA polymerase I inhibitor CX-5461 suppresses proliferation of vascular smooth muscle cells, mainly by inducing DNA damage response (DDR), including activations of ataxia telangiectasia mutated (ATM)/ATM and Rad3-related (ATR) and p53. Currently, there is no information about the molecular mechanism(s) underlying CX-5461-induced DDR in vascular cells, while the results obtained in cancer cells and immortalized cell lines are controversial. In this study, we examined the responses of various DDR pathways to CX-5461 treatment in primary aortic smooth muscle cells isolated from normal adult Sprague Dawley rats. We demonstrated that CX-5461-induced DDR was not associated with activations of the nucleotide excision repair, DNA mismatch repair, or the non-homologous end joining pathways, while the homologous recombination pathway was activated. However, the alkaline comet assay did not show massive DNA double strand breaks in CX-5461-treated cells.

Abbreviations: ATM, ataxia telangiectasia mutated; ATR, ATM and Rad3-related; DDR, DNA damage response; *Pol*I, RNA polymerase I; SMC, smooth muscle cells; MOVAS, mouse aortic SMC line; shRNA, short-hairpin RNA; SD, standard deviation; ANOVA, one-way analysis of variance; NER, nucleotide excision repair; HR, homologous recombination; DNA-PKcs, DNA-dependent protein kinase catalytic subunit; NHEJ, non-homologous end joining; PCNA, proliferating cell nuclear antigen; TIF-IA, transcription initiation factor-IA; NPM, nucleophosmin.

* Corresponding author. Department of Geriatric Medicine, Qilu Hospital of Shandong University, 107 Wen Hua Xi Road, Jinan, Shandong Province 250012, China.

*** Corresponding author. Department of Pharmacology, School of Basic Medical Sciences, Shandong University, 44 Wen Hua Xi Road, Jinan, Shandong Province 250012, China.

** Corresponding author. Department of Obstetrics and Gynecology, Qilu Hospital of Shandong University, 107 Wen Hua Xi Road, Jinan, Shandong Province 250012, China.

E-mail addresses: wangmaq@sdu.edu.cn (J. Wang), liuhuiqing@sdu.edu.cn (H. Liu), fjiang@sdu.edu.cn (F. Jiang).

[1] Current affiliation: Key Laboratory of Marine Drugs, Chinese Ministry of Education, School of Medicine and Pharmacy, Ocean University of China, Qingdao, Shandong Province, China.

[2] Current affiliation: Laboratory Medicine Center, The Second Hospital of Shandong University, Jinan, Shandong Province, China.

https://doi.org/10.1016/j.heliyon.2024.e37227
Received 10 February 2024; Received in revised form 28 August 2024; Accepted 29 August 2024
Available online 30 August 2024

Instead, CX-5461-induced DDR appeared to be related to induction of DNA replication stress, which was not attributable to increased formation of G-quadruplex or R-loop structures, but might be explained by the increased replication-transcription conflict. CX-5461-induced DDR was not exclusively confined to rDNA within the nucleolar compartment; the extra-nucleolar DDR might represent a distinct secondary response related to the downregulated Rad51 expression in CX-5461-treated cells. In summary, we suggest that DNA replication stress may be the primary molecular event leading to downstream ATM/ATR and p53 activations in CX-5461-treated vascular smooth muscle cells. Our results provide further insights into the molecular basis of the beneficial effects of CX-5461 in proliferative vascular diseases.

1. Introduction

CX-5461 is the first-in-class small molecule selective inhibitor of RNA polymerase I (*Pol*I), which is originally developed as a therapeutic agent to treat cancers [1,2]. Killing of proliferating cancer cells by CX-5461 is anticipated because, on the one hand, *Pol*I inhibition may suppress rRNA synthesis thereby restricting cellular ribosomal biogenesis and protein translation; on the other hand, *Pol*I inhibition induces nucleolar stress response in mammalian cells, which culminates in stabilization of the tumor suppressor p53 [3-6]. In fact, small-scale clinical trials have proved that CX-5461 exhibits promising therapeutic activities in both hematological and solid malignancies [7]. These studies have also demonstrated that CX-5461 is well-tolerated in patients and shows favorable short-term safety properties [8].

Previously, our group carried out a series of studies exploring the pharmacological effects of CX-5461 on several proliferative vascular disorders. We showed that CX-5461 treatment could effectively repress the development of intra-luminal injury-induced neointimal hyperplasia [9], ameliorate transplantation-induced vasculopathy [10], and retard the development of pulmonary arterial hypertension [11]. Moreover, CX-5461 displayed potent anti-fibrotic effects in cardiac fibroblasts [12]. Mechanistically, our results point to an important role of induction of p53 activation (phosphorylation on Ser15) in mediating the CX-5461 effects in cardiovascular cells, and activation of the ataxia telangiectasia mutated (ATM)/ATM and Rad3-related (ATR) pathway appears to lie upstream of p53 activation [9,11,12].

The canonical nucleolar stress response results in p53 stabilization by repressing Mdm2-mediated p53 ubiquitination and degradation [4,13]. However, our studies failed to demonstrate that CX-5461 increases the total amount of p53 in vascular cells. Instead, we and others have provided evidence showing that CX-5461 triggers activation of the ATM/ATR pathway [9,12,14,15], a key player in the DNA damage response (DDR) in eukaryotic cells [16,17]. At present, however, the molecular mechanisms underlying CX-5461-induced DDR are not clearly understood, while the results from different groups are controversial. Based on the data obtained in cancer cells and immortalized cell lines, four working models have been proposed. Firstly, CX-5461 displaces *Pol*I from the rDNA promoter, leading to stabilization of RNA:DNA hybrid structures known as R-loops [1,14,18]. Secondly, CX-5461 irreversibly locks the *Pol*I-containing preinitiation complex, which is non-functioning, on the rDNA [19]. Thirdly, CX-5461 stabilizes G-quadruplex structures formed in the genome in a rDNA-nonspecific manner [20]. Whichever mechanism is the case, the above models argue that disruption of normal DNA replication (*e.g.* replication fork stalling and fork collapse) is the final trigger of DDR induction [21]. Fourthly, CX-5461 induces DDR and p53 activation by altering the normal functioning of topoisomerase II [22].

It is noted that, in comparison to primary cells, cancer cell lines may be associated with known or unknown dysfunctions in DDR pathways [23]. Currently, however, there is little information about the potential molecular mechanism(s) of CX-5461-induced DDR in primary cells. Inspired by the above reports, and based on the ATM/ATR-p53 activating effects of CX-5461 observed in vascular smooth muscle cells (SMCs) and cardiac fibroblasts [9,11,12], in the present study we aim to characterize the responses of various DDR pathways to CX-5461 treatment in SMCs, and attempt to identify the upstream molecular events leading to the DDR induction.

2. Materials and methods

2.1. Cell culture

The use of experimental animals was approved by the Animal Ethics Committee of Shandong University School of Basic Medicine (Document #ECSBMSSDU-2017-050). All animal handling activities were carried out in accordance with the Guide for Care and Use of Laboratory Animals (NIH, 1996) and reported in accordance with the ARRIVE guidelines (https://arriveguidelines.org). Normal male Sprague Dawley rats were purchased from Vital River Laboratory (Beijing, China). Rats were maintained in a non-SPF grade facility, with an air-conditioned environment, 12-h light/dark cycles, and sterilized normal chow diet and tap water being given ad libitum. Rats of ~10 weeks of age were euthanized by intraperitoneal injection of overdose of pentobarbital sodium. Primary vascular SMCs were isolated from the aortas using explant-outgrowth method as described previously [24]. The thoracic aorta was removed and washed in sterile PBS containing penicillin (200 U/mL) and streptomycin (200 μg/mL) (Thermo Fisher, Waltham, MA, USA). After ripping off the adventitial fat and connective tissues, the aorta was cut open longitudinally. Under a dissection microscope, the intima was denuded by mechanical scratching, and the medial layer was resected carefully using fine forceps. The medial tissue was transferred to DMEM medium containing 20 % FBS (all from Thermo Fisher) and antibiotics, and cut into pieces of 1×1 mm^2. The tissue explants were seeded on a dry surface in a 25-cm^2 culture flask, and the flask was put in a standard 5 % CO_2 incubator for 4 h, letting

the tissues to adhere to the surface firmly. Then the tissues were immersed and cultured in the DMEM; the medium was changed every 3–5 days. The cell outgrowths from the explants were sub-cultured when 80 % confluence was reached, and maintained further in DMEM with 10 % FBS. For experimentations, cells below passage 10 were used. The mouse aortic SMC line (MOVAS) was originally purchased from ATCC (CRL-2797, Manassas, VA, USA), and maintained in DMEM with 10 % FBS.

2.2. Assessment of cell viability and proliferation

Cell viability and proliferation were assessed using colorimetric Enhanced Cell Counting Kit-8 (from Beyotime, Beijing, China). Primary SMCs were seeded in 96-well plates at an initial density of 1×10^4 cells per well; the end-point reading was acquired using an EMax Plus microplate reader (Molecular Devices, Sunnyvale, CA, USA) at 540 nm. For BrdU labeling assay, primary SMCs grown in 6-well plates to ~50 % confluence or over-confluence were labeled with BrdU (50 μM) at 37 °C for 3 h. Cells were briefly fixed with 4 % paraformaldehyde, denatured with 2 M HCl and treated with 0.1 M Na2B4O7 (pH 8.5). BrdU was detected with APC-conjugated anti-BrdU antibody (clone Bu20a) (#339807; RRID:AB_10900446, from BioLegend, San Diego, CA, USA) for 2 h at room temperature. The cells were analyzed using a Cytomics FC 500 cytometer (BD, Franklin Lakes, NJ, USA). The data were analyzed using FlowJo software (Becton, Dickinson and Company, Franklin Lakes, NJ, USA).

2.3. Immunofluorescence

Primary SMCs cultured on coverslips were fixed in 4 % paraformaldehyde for 30 min, and permeabilized with 0.5 % Triton X-100 for 15 min. The samples were blocked with 5 % bovine serum albumin, and incubated overnight with the primary antibody at 4 °C. After washing, the samples were incubated with CoraLite488-conjugated secondary antibodies (Proteintech, Wuhan, Hubei Province, China) and counter-stained with DAPI. Images of × 400 power were taken using a fluorescence microscope (Eclipse Ni-U, Nikon, Japan). For each slide, 3 to 5 high-power fields were randomly selected for analysis and the data were averaged. For categorical characterization, the cell nuclei were surveyed one by one, and the cells were classified as positive or negative depending on the presence or absence of the fluorescence signal. For analyzing the pattern of Rad51 foci, the nuclei were classified as null, medium (foci occupying less than 50 % of the total area of a nucleus), or high (foci occupying greater than 50 % of the total area of a nucleus). For numerical quantification, the mean fluorescence intensity (in arbitrary unit) was measured in individual nuclei using ImageJ software (NIH). The nucleolar stress response was assessed as described [25]. Briefly, the translocation of nucleophosmin (NPM), a nucleolar marker, from nucleoli to the nucleoplasm was detected by immunofluorescence labeling. The degree of nucleolar stress was expressed as the fluorescence intensity ratio between the 2 compartments. The morphological analysis was performed in a blind manner. The following antibodies were used for immunofluorescence staining: phospho-ATM (S794) (ab119799, RRID: AB_10938147), γH2AX (Ser139) (ab26350, RRID: AB_470861), DNA-PKcs (ab32566, RRID: AB_731981), Rad51 (ab133534, RRID: AB_2722613), fibrillarin (ab203400), and NPM (ab10530, RRID: AB_297271) were from Abcam (Cambridge, UK). Phospho-ATR (Ser428) (#2853, RRID: AB_2290281) and RPA32/RPA2 (#2208, RRID: AB_2238543) were from Cell Signaling Technology (Beverley, MA, USA). XPA (sc-28353, RRID: AB_628450) and MSH2 (sc-376384, RRID: AB_10988231) were from Santa Cruz Biotechnology (Dallas, TX, USA). Anti-DNA G-quadruplex (clone 1H6) (MABE1126) was from Millipore (Darmstadt, Germany). Anti-DNA-RNA Hybrid (clone S9.6) (ENH001, RRID: AB_2687463) was from Kerafast (Boston, MA, USA).

2.4. Immunoprecipitation

Primary SMCs were homogenized in cold lysis buffer containing 100 mM NaCl, 2 mM $MgCl_2$, 1 % Triton X-100, 20 mM HEPES (pH 7.4), and Protease Inhibitor Mixture (from Solarbio, Beijing, China). The protein concentration of samples was adjusted to 0.5 or 1.0 mg/mL. For immunoprecipitation, samples were precleared with normal IgG and Protein A/G agarose beads (from Cell Signaling), and incubated overnight with mouse anti-PCNA antibody (60097-1-Ig, RRID: AB_2236728, from Proteintech) at 4 °C with constant rotation. Negative control was performed by incubating with normal IgG. The samples were mixed with Protein A/G beads and further incubated at 4 °C for 4 h with constant rotation. The beads were washed and boiled in Laemmli loading buffer. Western blot detection was performed using a rabbit anti-ubiquitin antibody (10201-2-AP, RRID: AB_671515, from Proteintech).

2.5. Western blot

Total proteins were extracted in RIPA lysis buffer containing Protein Phosphatase Inhibitors cocktail and Protease Inhibitor Mixture (all from Solarbio). Samples were separated by SDS-PAGE and transferred to polyvinylidene fluoride membrane. The membrane was blocked with 5 % nonfat milk, incubated overnight with primary antibodies at 4 °C on an orbital shaker. Then the membrane was washed, incubated with horseradish peroxidase-conjugated secondary antibodies for 1 h at room temperature, and developed with Immobilon ECL Substrate (Merck-Millipore). Images were captured using a gel imaging instrument (ChemiDoc XRS+ from Bio-Rad, Hercules, CA, USA). Band densitometry analysis was performed using ImageJ. The following antibodies were used for Western blot: phospho-p53 (Ser15) (#9284, RRID: AB_331464), p53(#2524, RRID: AB_331743) and ATR (#13934, RRID: AB_2798347) were from Cell Signaling; GAPDH (10494-1-AP, RRID: AB_2263076) was from Proteintech.

2.6. Alkaline comet assay

Alkaline comet assay was performed using CometAssay Kit (Trevigen, Gaithersburg, MD, USA). Primary SMCs were detached and resuspended in cold PBS to a concentration of 10^5 cells/mL. An aliquot of 10 μL of the cell suspension was mixed with 100 μL of melted LM agarose (37 °C). The mixture was transferred onto a comet slide and allowed to solidify at 4 °C for 10 min. The cells were lysed in pre-chilled lysis solution for 60 min at 4 °C, and denatured at room temperature in an alkaline solution containing 300 mM NaOH and 1 mM EDTA for 60 min. Electrophoresis was carried out under 1 V/cm in a solution containing 300 mM NaOH and 1 mM EDTA for 30 min. All incubation and electrophoresis steps were performed in dark. The slides were stained with SYBR Green for 20 min and immediately photographed using the fluorescence microscope. The comet profile was quantitated using the Comet Assay Software Project tool (http://casp.sourceforge.net, RRID:SCR_007249).

2.7. Gene silencing

Lentiviral vectors expressing a short-hairpin RNA (shRNA) construct targeting murine TIF-IA (GCACAGACTGTCTTCCTTA) were purchased from Genepharma (Shanghai, China). A non-targeting shRNA (TTCTCCGAACGTGTCACGT) sequence was used as control. Twenty-four hours before lentiviral infection, MOVAS cells were sub-cultured into a 12-well plate (10^5 cells per well). Cells were incubated with 10^7 viral particles per well with 5 μg/mL of polybrene suspended in 0.5 mL of complete medium for 24 h. Then the cells were changed to fresh medium and further cultured for 2 days before subsequent experimentations.

2.8. Cell death analysis with propidium iodide staining

Cells seeded on coverslips were incubated with propidium iodide (#HY-D0815, from MedChemExpress, Monmouth Junction, NJ, USA) at a concentration of 5 μg/mL dissolved in culture medium, at 37 °C for 20 min in dark. After washing, cells were fixed in 4 % paraformaldehyde for 10 min at room temperature, and counterstained with DAPI. Images were captured with a fluorescence

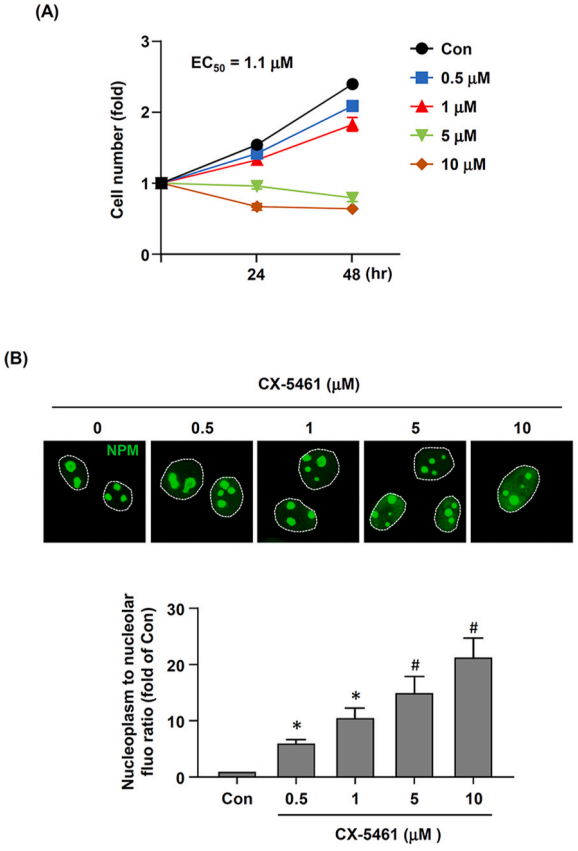

Fig. 1. Concentration-response relationships of CX-5461-induced effects on proliferation and nucleolar stress in rat primary vascular SMCs. (A) Effects of CX-5461 on cell proliferation detected using colorimetric Enhanced Cell Counting Kit-8 (n = 2–3). (B) Immunofluorescence staining for NPM and semi-quantitative data showing the effect of CX-5461 on induction of nucleolar stress response, assessed by the ratio of average fluorescence intensity in the nucleoplasm to that in the nucleoli. The location of nuclei was indicated by dashed lines. Data were expressed as mean ± SD. $^{\#}P < 0.05$ Kruskal-Wallis test; $^{*}P < 0.05$ ordinary one-way ANOVA, comparing *versus* control (Con), $n = 3$.

microscope. Cells with positive propidium iodide staining in the nuclei were counted as dead cells.

2.9. Measurement of lactate dehydrogenase release

Cellular toxicity was also assessed by measuring the release of lactate dehydrogenase (LDH). LDH concentrations in the culture medium were determined using LDH Cytotoxicity Assay Kit (purchased from Beyotime) according to the manufacturer's instructions.

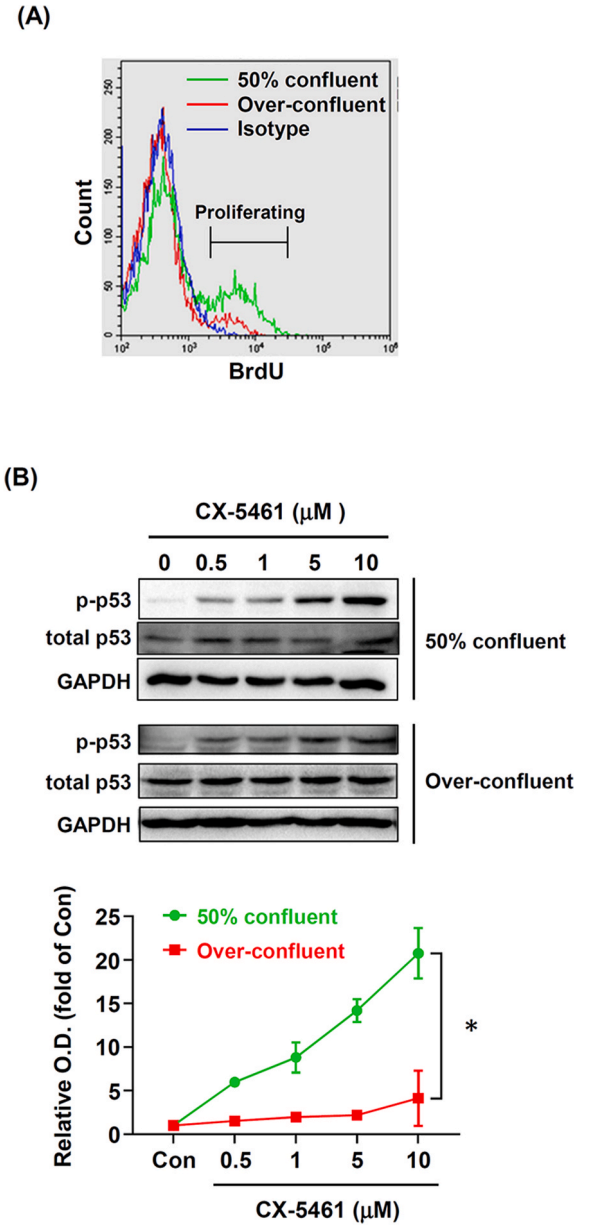

Fig. 2. Concentration-response relationship of CX-5461-induced p53 phosphorylation in proliferating and non-proliferating primary SMCs. (A) Representative flow cytometry results (from 2 independent tests of BrdU incorporation assay) showing the difference in the rate of proliferation between cells of ~50 % confluence and cells of over-confluence. (B) Representative western blots and quantitative densitometry data showing effects of CX-5461 on the level of p53 phosphorylation in proliferating (50 % confluent) and non-proliferating (over-confluent) cells. See Supplementary Original WB Pictures for the original uncropped blot images. Data were expressed as mean ± SD. *$P < 0.05$ for both concentration effect and proliferation status effect, two-way ANOVA ($n = 3$).

2.10. Statistical analysis

Data were reported as mean ± standard deviation (SD). Statistical analyses were performed using Prism software (Version 8.0) (GraphPad Software Inc, San Diego, CA, USA). For results with clear-cut differences, experiments were repeated 3 times. Comparisons between 2 groups with $n = 3$ were performed using unpaired *t*-test with Welch's correction, because non-parametric *t*-test was not suitable (rendering all results insignificant). For data with $n > 3$, non-parametric Mann-Whitney test was used. Multi-group data were tested using non-parametric analysis of variance (ANOVA) (Kruskal-Wallis test with False Discovery Rate correction). If no significance was detected, the data were reanalyzed using ordinary one-way ANOVA with *post hoc* Dunnett's test. Multi-group data with two variables were tested using two-way ANOVA. Data normality were tested using Shapiro-Wilk method. We confirmed that most of our data passed the normality test, with 2 exceptions which were indicated in the figure legends. Two-tailed P values < 0.05 were considered as statistically significant. The reported n values refereed to the number of independent experiments, but not number of technical replicates or number of selected multiple microscopic fields in each slide (for immunofluorescence assays).

3. Results

3.1. Concentration-response relationships of CX-5461-induced cellular effects in vascular SMCs

First we characterized the effective concentration ranges of CX-5461 which were able to inhibit proliferation of rat vascular SMCs and to induce nucleolar stress response. As shown in Fig. 1A, CX-5461 from 0.5 to 10 μM concentration-dependently reduced cell proliferation ($EC_{50} = 1.1$ μM), while at 10 μM CX-5461 exhibited moderate cytotoxicity (as evidenced by the decreased cell number to a level below baseline). Similarly, CX-5461 from 0.5 to 10 μM induced nucleolar stress response in SMCs (Fig. 1B). Next we tested the concentration-response relationship of CX-5461-induced p53 phosphorylation in proliferating and non-proliferating SMCs. Cells of ~50 % confluence maintained in normal culture medium were regarded as in proliferating status. To mimic a non-proliferating condition, cells were cultured until over-confluent confirmed by phase contrast microscopy. The reduced proliferating rate of the over-confluent cells was confirmed by flow cytometry (Fig. 2A). As shown in Fig. 2B (also see Supplementary Original WB Pictures),

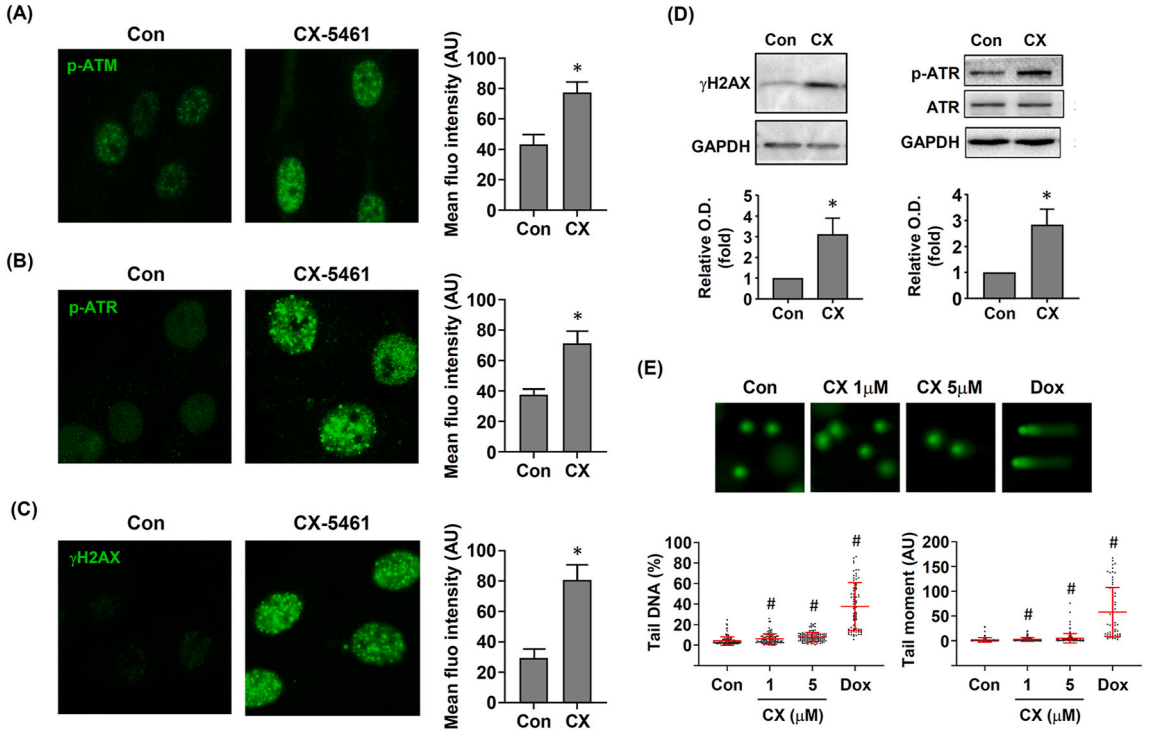

Fig. 3. CX-5461-induced DNA damage response in primary SMCs. (A to C) Immunofluorescence results showing that CX-5461 (1 μM for 24 h) significantly increased the levels of phospho-ATM, phospho-ATR, and γH2AX in the nuclei. (D) Representative western blots and densitometry data showing that CX-5461 significantly increased the levels of γH2AX and phospho-ATR. See Supplementary Original WB Pictures for the original uncropped blot images. (E) Representative images and quantitative data of alkaline comet assay showing the effect of CX-5461 on DNA stand breaks. Doxorubicin (Dox, 1 μM for 24 h) was used as positive control. Data were expressed as mean ± SD. For A to D, $^{*}P < 0.05$ *versus* Con, unpaired *t*-test ($n = 3$). For E, individual comet geometry data collected from 3 independent experiments were pooled and analyzed together (each point represented a single cell; bars represented mean ± SD). $^{\#}P < 0.05$ *versus* Con, Kruskal-Wallis test. AU, arbitrary unit. N.B. The data of CX-5461 group in 3C failed normality tests.

CX-5461 of 0.5–10 μM concentration-dependently increased the levels of p53 phosphorylation in both proliferating and non-proliferating cells, with the amplitude of response was greater in proliferating cells than non-proliferating cells. Based on the above data, we used 1 μM as a reference effective concentration of CX-5461 in the following experiments. The lack of cytotoxicity of 1 μM CX-5461 in primary SMCs was further confirmed by propidium iodide staining and LDH release (see Supplementary Fig. S1).

3.2. CX-5461 triggers DDR in SMCs

Previously we showed that CX-5461 could activate the ATM/ATR pathway in vascular SMCs [9]. Here we first confirmed that CX-5461 had a similar effect in primary SMCs under the present experimental setting, by showing that CX-5461 at 1 μM for 24 h significantly increased the levels of phospho-ATM and phospho-ATR in the nuclei (Fig. 3A and B). Next, we demonstrated that CX-5461 increased the abundance of nuclear γH2AX (Fig. 3C). We also confirmed the increased levels of γH2AX and phospho-ATR in CX-5461-treated cells with western blotting (Fig. 3D and Supplementary Original WB Pictures). Nevertheless, alkaline comet assay revealed that the accumulation of DNA double stand breaks in CX-5461-treated cells was not pronounced, in contrast to the effect of doxorubicin, a topoisomerase II inhibitor (Fig. 3E). Consistently, we showed that, unlike CX-5461, doxorubicin exhibited obvious cytotoxicity in primary SMCs (Supplementary Fig. S2).

3.3. Effects of CX-5461 on different DNA repair pathways

To understand the nature of CX-5461-triggered DDR in SMCs, we examined the markers of various DNA repair pathways. We found that CX-5461 treatment (1 μM for 24 h) did not induce significant nuclear accumulation of XPA (xeroderma pigmentosum group A) (Fig. 4A), a marker of the nucleotide excision repair (NER) pathway [26]. Similarly, CX-5461 did not induce the formation of MSH2

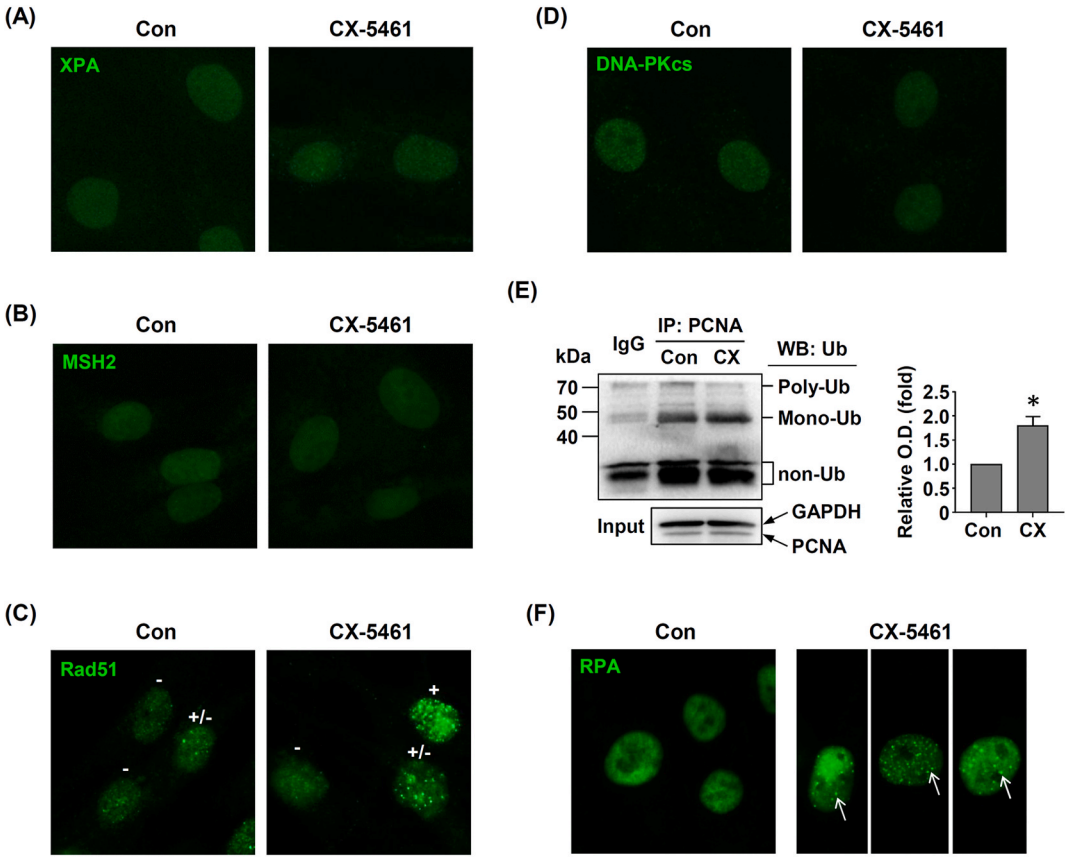

Fig. 4. Effects of CX-5461 on activation of different DNA repair pathways. (A to D) Representative images of immunofluorescence staining showing the effects of CX-5461 on markers of nucleotide excision repair, DNA mismatch repair, homologous recombination, and non-homologous end joining pathways. All of the targets exhibited clear nuclear localization. -, Rad51 foci null; ± Rad51 foci medium; +, Rad51 foci high. (E) Results of immunoprecipitation (IP) and western blotting (WB) showing changes in ubiquitination (Ub) of PCNA in CX-5461-treated cells. The quantitative densitometry data were for levels of mono-ubiquitination. PCNA = 29–31 kDa; Ub = 26 kDa. See Supplementary Original WB Pictures for the original uncropped blot images. (F) Immunofluorescent images showing that CX-5461 resulted in RPA foci formation in the nuclei (indicated by arrows). In the right panel, cells from different fields were grouped together. Data were expressed as mean ± SD. *$P < 0.05$ *versus* Con, unpaired *t*-test. All experiments were repeated 3 times.

foci in the nuclei [27], a marker of the DNA mismatch repair pathway (Fig. 4B). In comparison, CX-5461 increased the abundance of Rad51 foci in the nuclei [28] (% cells in CX-5461 group versus control group): Rad51 foci null 64.5 ± 6.9 *versus* 96. 7 ± 1.9; Rad51 foci medium 27.2 ± 4.6 *versus* 3.3 ± 1.9; Rad51 foci high 8.3 ± 2.9 *versus* 0, $P < 0.05$ one-way ANOVA, $n = 3$) (see Fig. 4C). These data indicated that there was an increased activation of the homologous recombination (HR) pathway. However, CX-5461 did not induce the formation of DNA-PKcs (DNA-dependent protein kinase catalytic subunit) foci (Fig. 4D), a marker of the non-homologous end joining (NHEJ) pathway [29,30]. Considering the weak effect of CX-5461 displayed in the comet assay, together with the lack of DNA-PKcs staining, we reasoned that the increased formation of Rad51 foci in CX-5461-treated cells was unlikely to be due to a significant accumulation of DNA double strand breaks, but might be related to the induction of replication stress, since the Rad51/HR axis was also involved in the protection/repairing of stalled replication forks [21,31]. To test this possibility, we performed immunoprecipitation assays, showing that CX-5461 treatment significantly increased the level of proliferating cell nuclear antigen (PCNA)

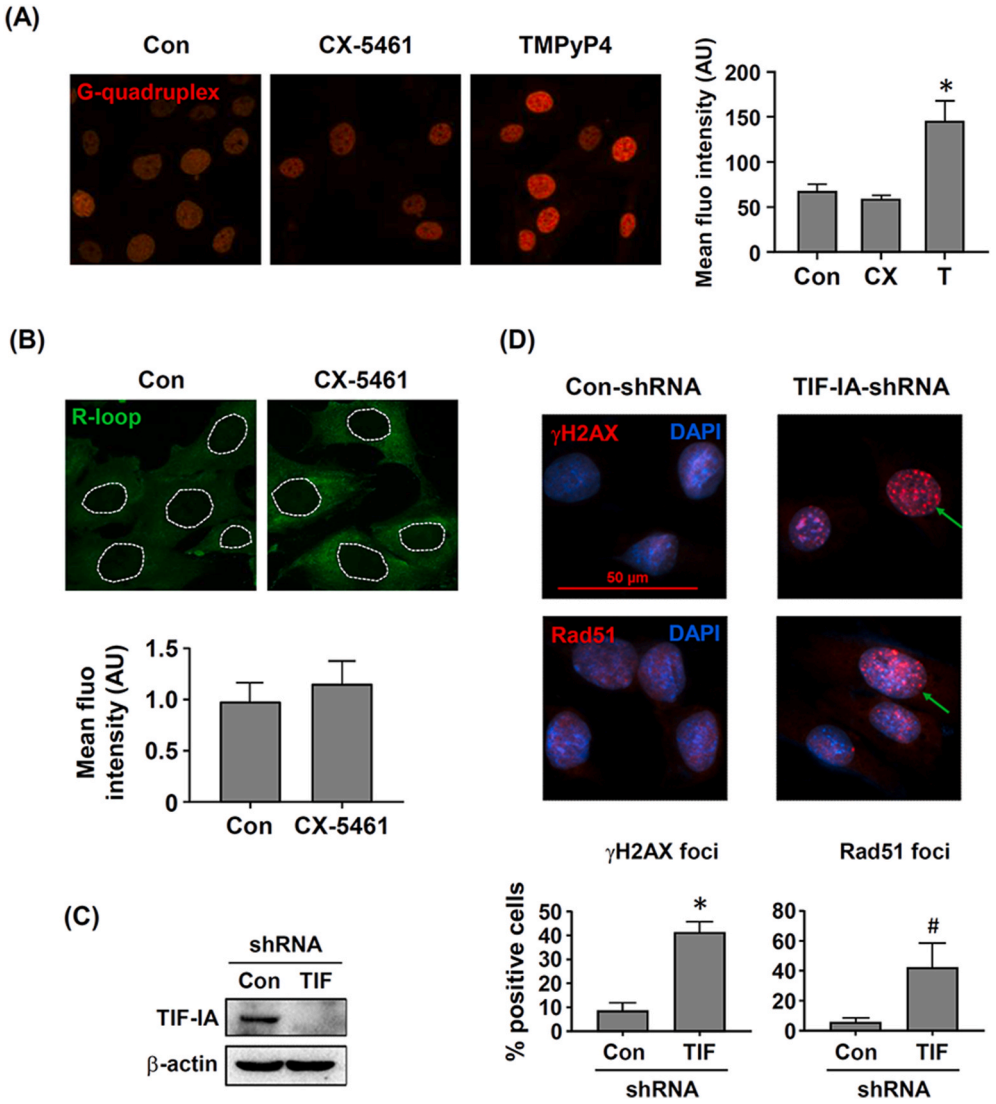

Fig. 5. CX-5461-induced DDR was not related to formation of G-quadruplexes or R-loops, but was mimicked by TIF-IA gene silencing. (A and B) Immunofluorescent images and quantitative data showing that CX-5461 had no significant effects on formation of G-quadruplexes or R-loops. Fluorescence intensity was measured in the nuclei (outlined in B), and expressed in arbitrary unit (AU). PC, positive control with TMPyP4 tosylate (T) treatment (10 μM for 24 h). (C) Western blots showing the gene silencing efficiency of the lentiviral vector expressing TIF-IA shRNA (example from 2 independent experiments). See Supplementary Original WB Pictures for the original uncropped blot images. (D) Immunofluorescent images and quantitative data showing that TIF-IA gene silencing increased the formation of γH2AX and Rad51 foci (indicated by arrows) in the nuclei (counter-stained with DAPI). Experiments in panels A and B were performed in primary SMCs; those in C and D were performed in MOVAS cell line. Data were expressed as mean ± SD. For A, $^{*}P < 0.05$ *versus* Con, only significant with ordinary one-way ANOVA ($n = 3$); for B, no significance with Mann-Whitney test ($n = 6$); for D left panel, $^{*}P < 0.05$ *versus* Con, unpaired *t*-test ($n = 3$); for D right panel, $^{\#}P < 0.05$ *versus* Con, Mann-Whitney test ($n = 4$). N.B. The data of CX-5461 group in 5A failed normality tests.

mono-ubiquitination (Fig. 4E and Supplementary Original WB Pictures), a marker of replication fork stalling [32]. Furthermore, using immunofluorescence microscopy, we detected the formation of replication protein A (RPA) foci in the nuclei, another marker of DNA replication stress [33]. RPA foci were absent in untreated cells, while CX-5461 treatment resulted in *de novo* RPA foci formation (Fig. 4F).

3.4. No evidence of increased formation of G-quadruplex or R-loop in CX-5461-treated cells

To clarify whether the increased induction of replication stress in CX-5461-treated SMCs was associated with formation of DNA G-quadruplexes as suggested by previous studies [20], we performed immunofluorescence labeling using the anti-G-quadruplex monoclonal antibody 1H6 [34]. The fluorescence signal of this antibody exhibited precise nuclear localization (Fig. 5A). However, we found that CX-5461 treatment had no effect on the intensity of G-quadruplex immunoreactivity (Fig. 5A). In contrast, treatment with TMPyP4 tosylate, a DNA G-quadruplex stabilizing ligand as a positive control [35], significantly increased the fluorescence signal in the nuclei (Fig. 5A). Apart from G-quadruplex, formation of R-loop structures was another important source of DNA replication stress. To test this possibility, we performed fluorescence labeling using an anti-DNA:RNA Hybrid monoclonal antibody S9.6. As reported by others [34], this antibody showed some background staining in the cytosol. Similar to the data in Fig. 5A, CX-5461 had no effect on the fluorescence intensity inside the nuclei (Fig. 5B).

Given that the G-quadruplex or R-loop structures were not implicated in CX-5461-induced effects, we wanted to further validate that the CX-5461 effects were indeed related to perturbation of the *Pol*I functioning. Hence we performed gene silencing for transcription initiation factor-IA (TIF-IA), a critical component of the *Pol*I machinery mediating the association between *Pol*I and the preinitiation complex [36,37] (Fig. 5C and Supplementary Original WB Pictures). It was demonstrated that depletion of TIF-IA mimicked the DDR-inducing effects of CX-5461, as evidenced by the increased formation of γH2AX and Rad51 foci (Fig. 5D). The above results together indicated that CX-5461 could trigger replication stress and DDR without inducing G-quadruplex or R-loop formation. We therefore reasoned that the model proposed by Mars et al. [19], in which *Pol*I was irreversibly locked by CX-5461 to the rDNA promoter in a non-functioning mode, provided a more plausible explanation to the observed actions of the agent in SMCs. To strengthen this argument, we tested the reversibility of CX-5461-induced effect on SMC proliferation. We treated the cells with CX-5461, H_2O_2 or doxorubicin for 24 h, washed off the compounds, and allowed the cells to recover for 24 h in fresh medium. Then the cells were sub-cultured to the same cell density, and allowed to attach for 24 h. After these procedures, we monitored the cell growth over 4 days. We found that both H_2O_2 or doxorubicin exhibited acute cytotoxicity; however, the surviving cells partly resumed the proliferation capability in the absence of the compounds. In comparison, cells with CX-5461 treatment could proliferate at a reduced rate within the first 48 h; strikingly, from 72 h the cells gradually stopped to proliferate even in the absence of CX-5461, and remained to be dormant throughout the 4-day period (Fig. 6 and Supplementary Fig. S3).

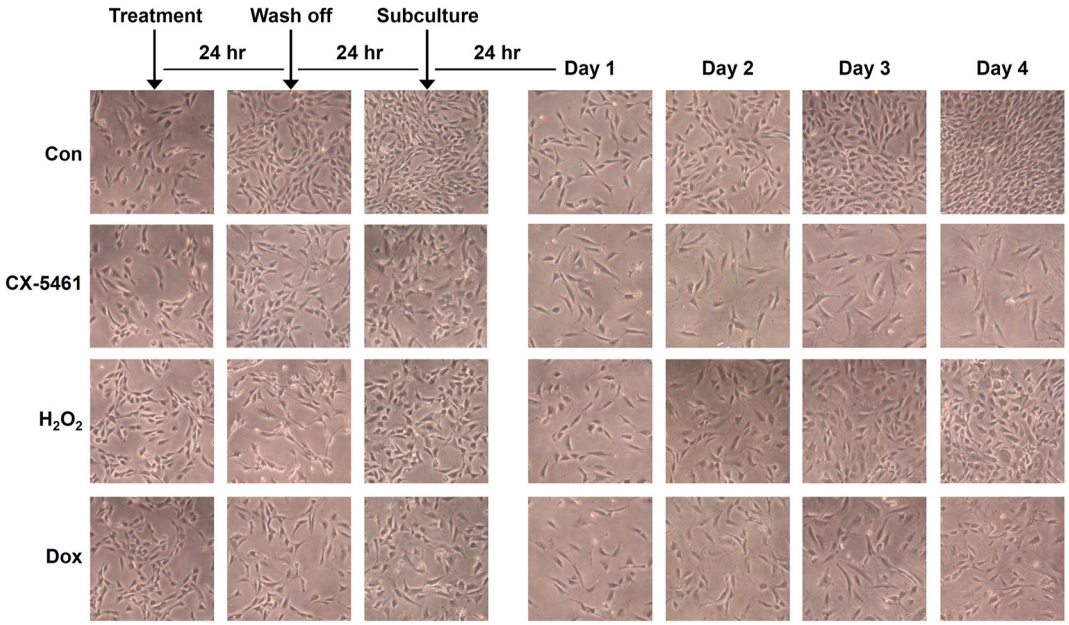

Fig. 6. Reversibility of the inhibitory effects induced by various stress inducers on SMC proliferation. Phase-contrast microscopy images of primary SMCs in culture were taken at various time points as indicated, showing the cell proliferative status under different treatment conditions. CX-5461, H_2O_2 and Dox were used at 1, 150 and 1 μM respectively. The quantitative data were given in Supplementary Fig. S3.

3.5. Inhibition of ATM/ATR blunts CX-5461-induced p53 phosphorylation

ATM/ATR are pivotal mediators in the HR pathway [16], we examined whether blocking ATM/ATR could blunt CX-5461-induced p53 phosphorylation. In Supplementary Fig. S4 (also see Supplementary Original WB Pictures), using immunofluorescence staining and western blotting, we demonstrated that combined treatment with the ATM inhibitor KU-55933 (1 μM) and ATR inhibitor VE-821 (0.5 μM) significantly attenuated p53 phosphorylation induced by CX-5461. In contrast, inhibition of DNA-PK (mediator of the NHEJ pathway) [16] with KU-57788 (1 μM) failed to modify the response of p53 phosphorylation. These data support the notion that activation of the HR pathway is essential in CX-5461-induced DDR and downstream effects.

3.6. CX-5461-induced DDR was not exclusively confined to rDNA

To clarify whether CX-5461-induced DDR was exclusively confined to rDNA within the nucleoli, we performed double immunofluorescence labeling assays using NPM or fibrillarin as nucleolar markers. We found that some of the CX-5461-induced γH2AX, Rad51 and phospho-ATR foci showed co-localization with the nucleolar markers; however, γH2AX, Rad51 and phospho-ATR signals were also present outside the nucleolar compartment (Fig. 7A). The mechanism of this phenomenon was not understood. Interestingly, we found that treatment with CX-5461 readily resulted in a decrease in the expression of Rad51 (Fig. 7B and C and Supplementary Original WB Pictures). We postulated therefore that the DDR induced by CX-5461 in the non-rDNA genome might be a secondary

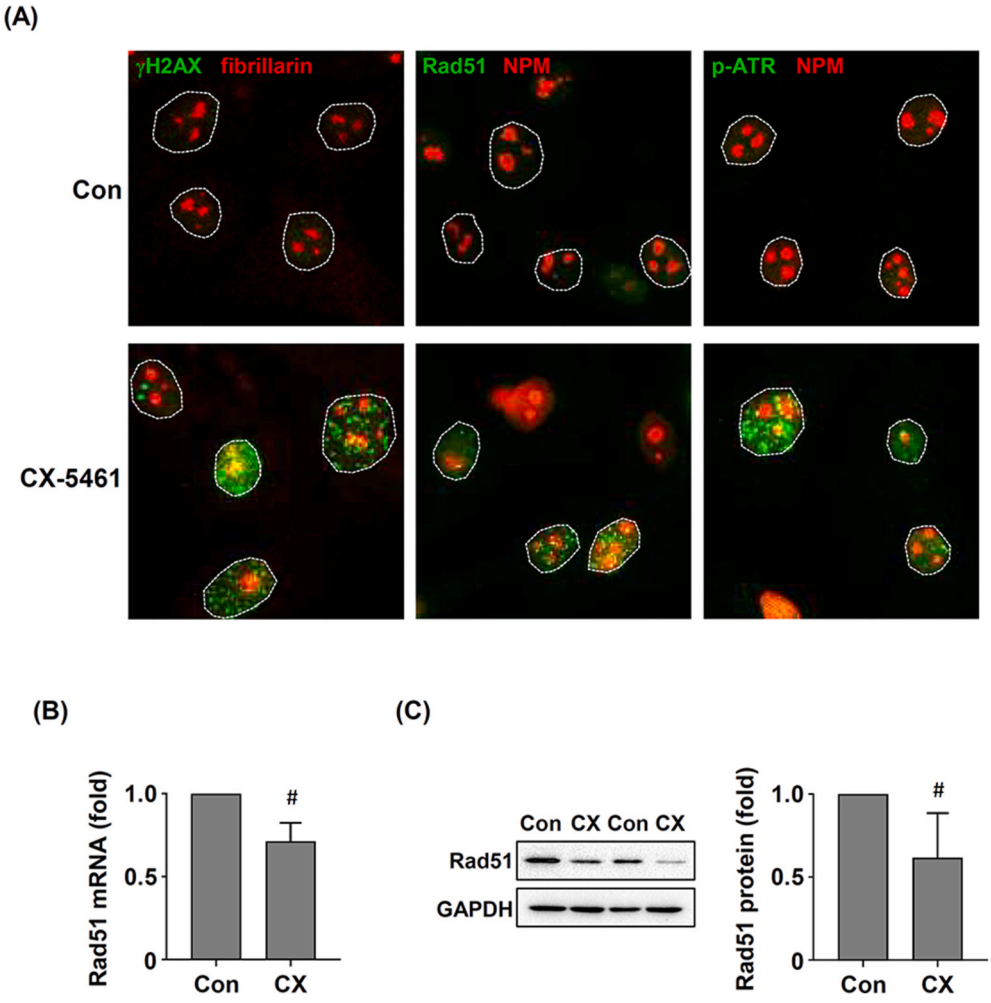

Fig. 7. CX-5461-induced DDR was not exclusively confined to rDNA in primary SMCs. (A) Double immunofluorescence labeling results showing that some of the CX-5461-induced γH2AX, Rad51 and phospho-ATR foci (green) exhibited co-localization with nucleolar markers (NPM or fibrillarin, red), while the green fluorescence signals were also present outside the nucleolar compartment. The nuclei were outlined. The images were example from 3 independent experiments. (B and C) qPCR and western blotting results showing that treatment with CX-5461 (1 μM for 24 h) significantly decreased the expression level of Rad51. See Supplementary Original WB Pictures for the original uncropped blot images. Data were expressed as mean ± SD. $^{\#}P < 0.05$ *versus* Con, Mann-Whitney test ($n = 4$).

response related to the reduction in Rad51 availability (see Discussion).

4. Discussion

Our previous studies have shown that in vascular SMCs, cardiac fibroblasts and primary monocytes/macrophages, CX-5461 at concentrations around 1 μM does not cause significant cell apoptosis, but instead triggers cell cycle arrest, thereby inhibiting cell proliferation [9,10,12]. In accordance with these results, we have repeatedly demonstrated that CX-5461 induces p53 Serine15 phosphorylation, but has minor effects on the total amount of p53 protein. The p53-activating property of CX-5461 is associated with several beneficial effects in the cardiovascular system *in vivo*, including repression of proliferative vascular remodeling caused by different etiologies, and possibly inhibition of cardiac fibrosis [9,10,12]. Moreover, our recent study has demonstrated that CX-5461-induced p53 activation effectively inhibits T cell-mediated alloimmunity and acute rejections following solid organ transplantation, indicating that the compound may represent a novel immunosuppressant [38]. Although the molecular mechanisms underlying the cytostatic effects of CX-5461 are not clearly understood, different lines of evidence (including that from our own studies) suggest that activation of ATM and/or ATR kinases may play important roles in mediating the cellular effects of CX-5461 [9,12,14,15]. In the present study in primary SMCs, we have confirmed that CX-5461, at a non-toxic concentration (1 μM) which effectively suppresses cell proliferation and stimulates p53 phosphorylation, elicits DDR in the cell as evidenced by the increased phosphorylation of ATM/ATR and H2AX.

Subsequently, we carried out experiments attempting to delineate the molecular basis of CX-5461-induced DDR in SMCs. Our data described in Fig. 4 ruled out the involvement of NER or DNA mismatch repair pathways. NHEJ and HR, two principal mechanisms responsible for repairing DNA double strand breaks, were differentially affected by CX-5461. Specifically, the NHEJ pathway was relatively insensitive to CX-5461 treatment, whereas the HR pathway was activated by CX-5461. The weak effect of CX-5461 revealed by comet assay and the lack of DNA-PKcs staining in CX-5461-treated cells together suggest that CX-5461-induced DDR is not primarily attributable to the accumulation of massive DNA double strand breaks. Instead, the concomitant activation of Rad51/HR axis, increase in RPA foci formation, and induction of PCNA mono-ubiquitination strongly suggest that CX-5461 causes replication stress [21,31]. It is well established that activation of ATR and its downstream effectors can stabilize and help restarting the stalled replication forks, avoiding the occurrence of genome instability [39]. Also, there is evidence showing that replication stress can activate the ATM kinase via PCNA mono-ubiquitination [40]. However, a limitation of the present study was that we did not provide a direct measurement on the DNA replication velocity (such as the Fluorescent DNA Fiber Analysis technique) in untreated and CX-5461-treated cells.

Disruption of the replication fork progression may be caused by multiple reasons, such as presence of DNA lesions, formation of unusual DNA structures, conflicts between replication and transcription, limitation of essential replication factors, and chromatin inaccessibility [39]. Our results indicate that in vascular SMCs, increased formation of G-quadruplex or R-loop structures is unlikely to have a major contribution to CX-5461-induced DDR. Either, CX-5461-induced DDR in SMCs is unlikely to be due to topoisomerase II poisoning as suggested by findings obtained in various cancer cell lines [22], because of the contrasting effects of CX-5461 and doxorubicin on cell viability and accumulation of DNA double strand breaks in primary SMCs. Indeed, it has been recognized that the rDNA genome is relatively unstable, because the high demand for rDNA transcription and the repetitive nature of rDNA significantly increase the risk of replication-transcription conflict and resultant replication fork stalling [41]. According to the model proposed by Mars et al. [19], if CX-5461 irreversibly locks *PolI* to the rDNA promoter, this effect can drastically increase the incidence of replication-transcription conflict in proliferating cells. This model is supported by our results in two aspects: (1) as shown by the wash-off experiments, after a transient pre-treatment with CX-5461, cells remain dormant after a prolonged period of recovery, when cell division is well resumed in H_2O_2- and doxorubicin-treated cells, indicating the irreversible nature of CX-5461 effect; (2) CX-5461-induced p53 phosphorylation is greater in proliferating cells than that in non-proliferating cells, indicating an impact possibly stemming from the DNA replication process. Moreover, if CX-5461-induced replication stress is caused by ligand-dependent formation of DNA lesions or aberrant secondary structures, the final DDR-inducing effect of CX-5461 should not be mimicked by depletion of TIF-IA, which mediates the binding between *PolI* and the preinitiation complex [36,37]. Nevertheless, we have repeatedly observed that TIF-IA depletion can mimic the DDR-inducing effect of CX-5461 in vascular SMCs [42]. Overall, we argue that the model proposed by Mars et al. [19] provides a more plausible explanation to the observed actions of CX-5461 in SMCs.

Interestingly, it is noted that CX-5461-induced DDR is not exclusively confined to rDNA within the nucleoli. We suggest that this phenomenon may represent a separate secondary response which is distinct from the primary DDR in CX-5461-treated cells as discussed above. Previous studies have shown that depletion of Rad51 *per se*, without additional stress inducers, can trigger DDR in cells with increased DNA replication challenges [43,44]. Also, there is evidence showing that pharmacological inhibition of Rad51 can trigger replication catastrophe in tumor cells [45]. These data suggest that maintaining a stable basal level of Rad51 is essential for maintaining genome stability. More importantly, increasing evidence suggests that, in addition to mediating HR processes during DNA repair, Rad51 also has a pivotal role in the protection of stalled, but unbroken, replication forks, and the latter function does not require its recombinase activity [31]. In light of these data, together with our observation that CX-5461 treatment decreases the expression level of Rad51, we argue that the DDR occurring outside the nucleolar compartment might be a manifestation of stochastic DNA damages aggravated by the reduced Rad51 availability in CX-5461-treated cells. However, the mechanism by which CX-5461 modulates Rad51 expression remains to be clarified.

In summary, the present study suggests that increased DNA replication stress may be the primary molecular event leading to downstream ATM/ATR and p53 activation in CX-5461-treated vascular smooth muscle cells. Our results provide further insights into the molecular basis of the observed beneficial effects of CX-5461 on proliferative vascular diseases.

Ethics statement

The use of experimental animals was approved by the Animal Ethics Committee of Shandong University School of Basic Medicine (Document #ECSBMSSDU-2017-050). All animal handling activities were carried out in accordance with the Guide for Care and Use of Laboratory Animals (NIH, 1996) and reported in accordance with the ARRIVE guidelines (https://arriveguidelines.org).

Data availability statement

All original data used to create the graphs were provided as Supplementary Materials (Source Data.xlsx).

CRediT authorship contribution statement

Tengfei Liu: Investigation, Formal analysis, Data curation. **Guopin Pan:** Investigation, Data curation. **Jing Zhang:** Investigation, Data curation. **Jianli Wang:** Methodology, Formal analysis. **Xiaosun Guo:** Writing – review & editing, Supervision, Project administration. **Ye Chen:** Investigation, Data curation. **Xiaoyun Wang:** Investigation, Data curation. **Xiaopei Cui:** Supervision, Data curation. **Huiqing Liu:** Writing – review & editing, Supervision, Project administration. **Fan Jiang:** Writing – review & editing, Writing – original draft, Supervision, Conceptualization.

Declaration of competing interest

The authors declare the following financial interests/personal relationships which may be considered as potential competing interests:Fan Jiang reports financial support was provided by National Natural Science Foundation of China. Jianli Wang reports financial support was provided by National Natural Science Foundation of China. If there are other authors, they declare that they have no known competing financial interests or personal relationships that could have appeared to influence the work reported in this paper.

Acknowledgements

The authors thank Jie Wang and Chaochao Dai for technical assistances. This study was partly supported by research grants from National Natural Science Foundation of China (#82070265 for F.J. and #81970347 for J.W.).

Appendix A. Supplementary data

Supplementary data to this article can be found online at https://doi.org/10.1016/j.heliyon.2024.e37227.

References

[1] D. Drygin, A. Lin, J. Bliesath, et al., Targeting RNA polymerase I with an oral small molecule CX-5461 inhibits ribosomal RNA synthesis and solid tumor growth, Cancer Res. 71 (4) (2011) 1418–1430.
[2] M. Haddach, M.K. Schwaebe, J. Michaux, et al., Discovery of CX-5461, the first direct and selective inhibitor of RNA polymerase I, for cancer therapeutics, ACS Med. Chem. Lett. 3 (7) (2012) 602–606.
[3] R.Y. Tsai, T. Pederson, Connecting the nucleolus to the cell cycle and human disease, Faseb j. 28 (8) (2014) 3290–3296.
[4] S. Boulon, B.J. Westman, S. Hutten, F.M. Boisvert, A.I. Lamond, The nucleolus under stress, Mol Cell 40 (2) (2010) 216–227.
[5] K. Yang, J. Yang, J. Yi, Nucleolar Stress: hallmarks, sensing mechanism and diseases, Cell Stress 2 (2018) 125–140.
[6] M.J. Bywater, R.B. Pearson, G.A. McArthur, R.D. Hannan, Dysregulation of the basal RNA polymerase transcription apparatus in cancer, Nat. Rev. Cancer 13 (5) (2013) 299–314.
[7] R. Ferreira, J.S. Schneekloth Jr., K.I. Panov, K.M. Hannan, R.D. Hannan, Targeting the RNA polymerase I transcription for cancer therapy comes of age, Cells 9 (2) (2020) 266.
[8] A. Khot, N. Brajanovski, D.P. Cameron, et al., First-in-Human RNA polymerase I transcription inhibitor CX-5461 in patients with advanced hematologic cancers: results of a phase I dose-escalation study, Cancer Discov. 9 (8) (2019) 1036–1049.
[9] Q. Ye, S. Pang, W. Zhang, et al., Therapeutic targeting of RNA polymerase I with the small-molecule CX-5461 for prevention of arterial injury-induced neointimal hyperplasia, Arterioscler. Thromb. Vasc. Biol. 37 (3) (2017) 476–484.
[10] C. Dai, M. Sun, F. Wang, et al., The selective RNA polymerase I inhibitor CX-5461 mitigates neointimal remodeling in a modified model of rat aortic transplantation, Transplantation 102 (10) (2018) 1674–1683.
[11] X. Xu, H. Feng, C. Dai, et al., Therapeutic efficacy of the novel selective RNA polymerase I inhibitor CX-5461 on pulmonary arterial hypertension and associated vascular remodeling, Br. J. Pharmacol. 178 (7) (2021) 1605–1619.
[12] S. Pang, Y. Chen, C. Dai, et al., Anti-fibrotic effects of p53 activation induced by RNA polymerase I inhibitor in primary cardiac fibroblasts, Eur. J. Pharmacol. 907 (2021) 174303.
[13] Y. Zhang, H. Lu, Signaling to p53: ribosomal proteins find their way, Cancer Cell 16 (5) (2009) 369–377.
[14] J. Quin, K.T. Chan, J.R. Devlin, et al., Inhibition of RNA polymerase I transcription initiation by CX-5461 activates non-canonical ATM/ATR signaling, Oncotarget 7 (31) (2016) 49800–49818.
[15] S.S. Negi, P. Brown, rRNA synthesis inhibitor, CX-5461, activates ATM/ATR pathway in acute lymphoblastic leukemia, arrests cells in G2 phase and induces apoptosis, Oncotarget 6 (20) (2015) 18094–18104.
[16] A.V. Shah, M.R. Bennett, DNA damage-dependent mechanisms of ageing and disease in the macro- and microvasculature, Eur. J. Pharmacol. 816 (2017) 116–128.

[17] A.M. Weber, A.J. Ryan, ATM and ATR as therapeutic targets in cancer, Pharmacol. Ther. 149 (2015) 124–138.
[18] E. Sanij, K.M. Hannan, J. Xuan, et al., CX-5461 activates the DNA damage response and demonstrates therapeutic efficacy in high-grade serous ovarian cancer, Nat. Commun. 11 (1) (2020) 2641.
[19] J.C. Mars, M.G. Tremblay, M. Valere, et al., The chemotherapeutic agent CX-5461 irreversibly blocks RNA polymerase I initiation and promoter release to cause nucleolar disruption, DNA damage and cell inviability, NAR Cancer 2 (4) (2020) zcaa032.
[20] H. Xu, M. Di Antonio, S. McKinney, et al., CX-5461 is a DNA G-quadruplex stabilizer with selective lethality in BRCA1/2 deficient tumours, Nat. Commun. 8 (2017) 14432.
[21] R.M. Jones, E. Petermann, Replication fork dynamics and the DNA damage response, Biochem. J. 443 (1) (2012) 13–26.
[22] P.M. Bruno, M. Lu, K.A. Dennis, et al., The primary mechanism of cytotoxicity of the chemotherapeutic agent CX-5461 is topoisomerase II poisoning, Proc Natl Acad Sci U S A. 117 (8) (2020) 4053–4060.
[23] M.J. O'Connor, Targeting the DNA damage response in cancer, Mol Cell 60 (4) (2015) 547–560.
[24] S. Xu, J. Fu, J. Chen, et al., Development of an optimized protocol for primary culture of smooth muscle cells from rat thoracic aortas, Cytotechnology 61 (1–2) (2009) 65–72.
[25] X. Bi, Q. Ye, D. Li, et al., Inhibition of nucleolar stress response by Sirt1: a potential mechanism of acetylation-independent regulation of p53 accumulation, Aging Cell 18 (2) (2019) e12900.
[26] X. Wu, S.M. Shell, Y. Liu, Y. Zou, ATR-dependent checkpoint modulates XPA nuclear import in response to UV irradiation, Oncogene 26 (5) (2007) 757–764.
[27] D. Zink, C. Mayr, C. Janz, L. Wiesmüller, Association of p53 and MSH2 with recombinative repair complexes during S phase, Oncogene 21 (31) (2002) 4788–4800.
[28] L. Li, K. Biswas, L.A. Habib, et al., Functional redundancy of exon 12 of BRCA2 revealed by a comprehensive analysis of the c.6853A>G (p.I2285V) variant, Hum. Mutat. 30 (11) (2009) 1543–1550.
[29] A.S. Gustafsson, A. Abramenkovs, B. Stenerlöw, Suppression of DNA-dependent protein kinase sensitize cells to radiation without affecting DSB repair, Mutat. Res. 769 (2014) 1–10.
[30] K. Maliszewska-Olejniczak, A. Dróżdż, M. Waluś, M. Dorosz, M.A. Gryziński, Immunofluorescence imaging of DNA damage and repair foci in human colon cancer cells, J. Vis. Exp. 160 (2020) e61399.
[31] I.E. Wassing, F. Esashi, RAD51: beyond the break, Semin. Cell Dev. Biol. 113 (2021) 38–46.
[32] J.T. Fox, K.Y. Lee, K. Myung, Dynamic regulation of PCNA ubiquitylation/deubiquitylation, FEBS Lett. 585 (18) (2011) 2780–2785.
[33] C. Coulson-Gilmer, R.D. Morgan, L. Nelson, et al., Replication catastrophe is responsible for intrinsic PAR glycohydrolase inhibitor-sensitivity in patient-derived ovarian cancer models, J. Exp. Clin. Cancer Res. 40 (1) (2021) 323.
[34] A. Henderson, Y. Wu, Y.C. Huang, et al., Detection of G-quadruplex DNA in mammalian cells, Nucleic Acids Res. 42 (2) (2014) 860–869.
[35] T. Lemarteleur, D. Gomez, R. Paterski, E. Mandine, P. Mailliet, J.F. Riou, Stabilization of the c-myc gene promoter quadruplex by specific ligands' inhibitors of telomerase, Biochem. Biophys. Res. Commun. 323 (3) (2004) 802–808.
[36] N. Hein, K.M. Hannan, A.J. George, E. Sanij, R.D. Hannan, The nucleolus: an emerging target for cancer therapy, Trends Mol. Med. 19 (11) (2013) 643–654.
[37] R. Jin, W. Zhou, Tif-Ia, An oncogenic target of pre-ribosomal RNA synthesis, Biochim. Biophys. Acta 1866 (2) (2016) 189–196.
[38] G. Pan, J. Zhang, Y. Han, et al., CX-5461 is a potent immunosuppressant which inhibits T cell-mediated alloimmunity via p53-DUSP5, Pharmacol. Res. 177 (2022) 106120.
[39] M.K. Zeman, K.A. Cimprich, Causes and consequences of replication stress, Nat. Cell Biol. 16 (1) (2014) 2–9.
[40] N. Kanu, T. Zhang, R.A. Burrell, et al., RAD18, WRNIP1 and ATMIN promote ATM signalling in response to replication stress, Oncogene 35 (30) (2016) 4009–4019.
[41] D. Salim, J.L. Gerton, Ribosomal DNA instability and genome adaptability, Chromosome Res. 27 (1–2) (2019) 73–87.
[42] W. Zhang, W. Cheng, R. Parlato, et al., Nucleolar stress induces a senescence-like phenotype in smooth muscle cells and promotes development of vascular degeneration, Aging (Albany NY) 12 (21) (2020) 22174–22198.
[43] J. Hu, Z. Zhang, L. Zhao, L. Li, W. Zuo, L. Han, High expression of RAD51 promotes DNA damage repair and survival in KRAS-mutant lung cancer cells, BMB Rep 52 (2) (2019) 151–156.
[44] L. Xu, T. Wu, S. Lu, et al., Mitochondrial superoxide contributes to oxidative stress exacerbated by DNA damage response in RAD51-depleted ovarian cancer cells, Redox Biol. 36 (2020) 101604.
[45] K. Mills, A. Cyr, T. Maclay, M. Day, M.G. Hasham, A. Khalil, A small molecule RAD51 inhibitor preferentially affects cells expressing high cytidine deaminase activity, Blood 130 (Supplement 1) (2017) 4627.